Electronic Supplementary Information

Enhanced constraint and catalysed conversion of lithium polysulfides via composite oxides from spent layered cathode

Wenze Yin,[a] Zhenguo Wu,[a] Wen Tian,[a] Yanxiao Chen,[a] Wei Xiang,[d] Guilin Feng,[a] Yongchun Li,[a] Chunjin Wu,[a] Chunliu Xu,[a] Changjiang Bai,[ac] Benhe Zhong,[a] Xinlong Wang,[*a] Jun Zhang,[c] Fengrong He,[c] Abdulmohsen Ali Alshehri[e] and Xiaodong Guo[ab]

[a]College of Chemical Engineering, Sichuan University, Chengdu 610065, PR China.
Email: wangxl@scu.edu.cn;
[b]Institute for Superconducting and Electronic Materials, University of Wollongong, Wollongong, NSW 2522, Australia;
[c]Dongguan Hec Technology Research Corporation, Guangdong, Dongguan, 523871, PR China;
[d]College of Materials and Chemistry &Chemical Engineering, Chengdu University of Technology, Chengdu 610059, PR China;
[e]Chemistry Department, Faculty of Science, King Abdulaziz University, P.O. Box 80203, Jeddah 21589, Saudi Arabia

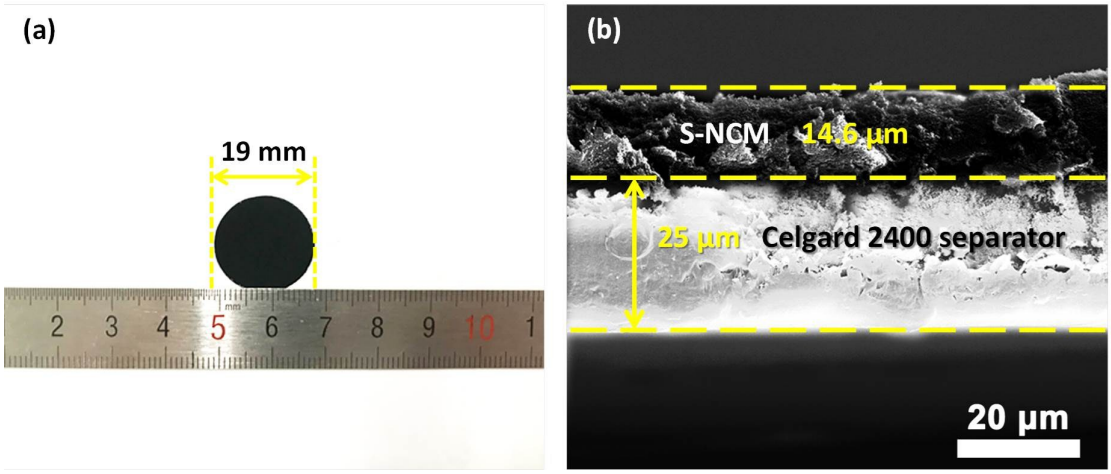

Fig. S1 (a) Digital photographs and (b) the cross-sectional morphology of the coated separator.

Table S1 Detailed experimental data for testing porosity.

	Celgard (mg)	Celgard after alcohol immersion (mg)	Coated separator (mg)	Coated separator after alcohol immersion (mg)
experiment 1	3.38	22.60	5.64	24.89
experiment 2	3.38	22.62	5.64	24.91
experiment 3	3.38	22.58	5.64	24.90
average	3.38	22.60	5.64	24.90

Table S2 ICP Results of S-NCM and C-NCM Particles.

specimen	NCM 523
S-NCM	$Li_{0.8117}Ni_{0.505}Co_{0.2008}Mn_{0.294}O_{2.012}$
C-NCM	$Li_{1.005}Ni_{0.496}Co_{0.206}Mn_{0.303}O_{2.013}$

Table S3 Lattice Parameters of S-NCM and C-NCM Particles.

specimen	a (Å)	c (Å)	V (Å^3)	I(003)/I(104)
S-NCM	2.892645	14.299911	103.622578	1.178
C-NCM	2.868350	14.248549	101.523235	1.566

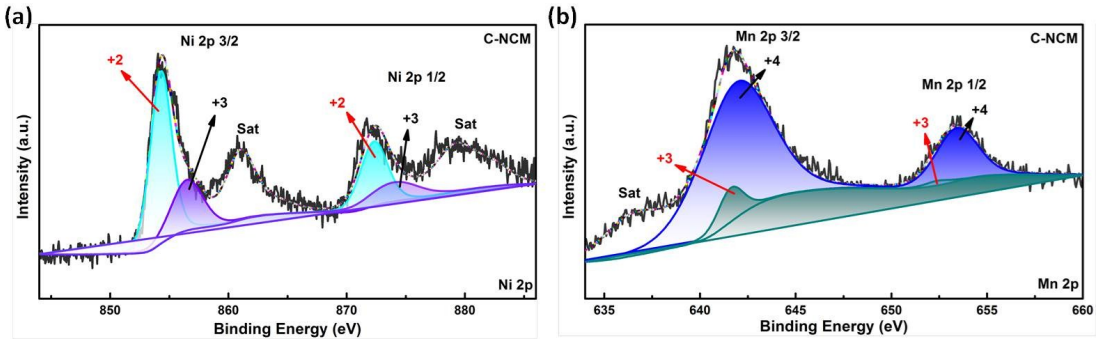

Fig. S2 XPS spectrum for (a) Ni 2p and (b) Mn 2p in the C-NCM.

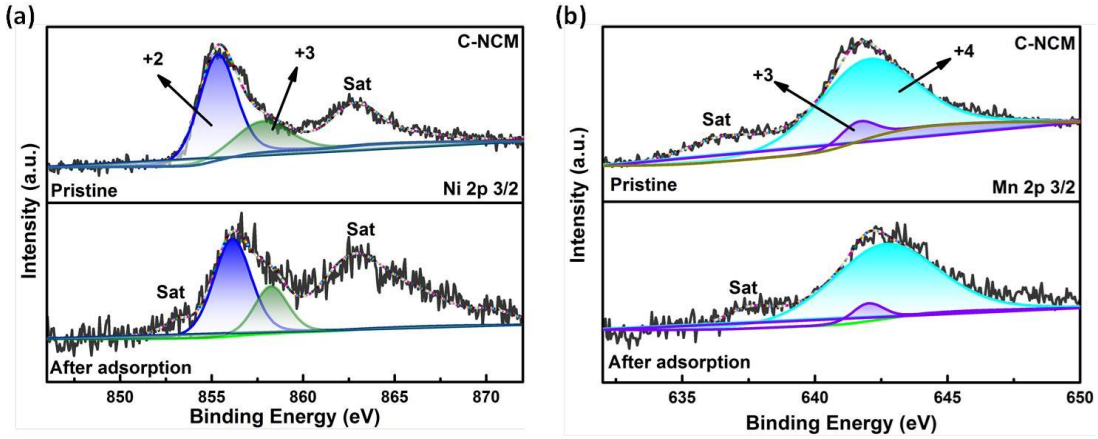

Fig. S3 High-resolution XPS spectra of (a) Ni $2p_{3/2}$ and (b) Mn $2p_{3/2}$ of the C-NCM before and after adsorption.

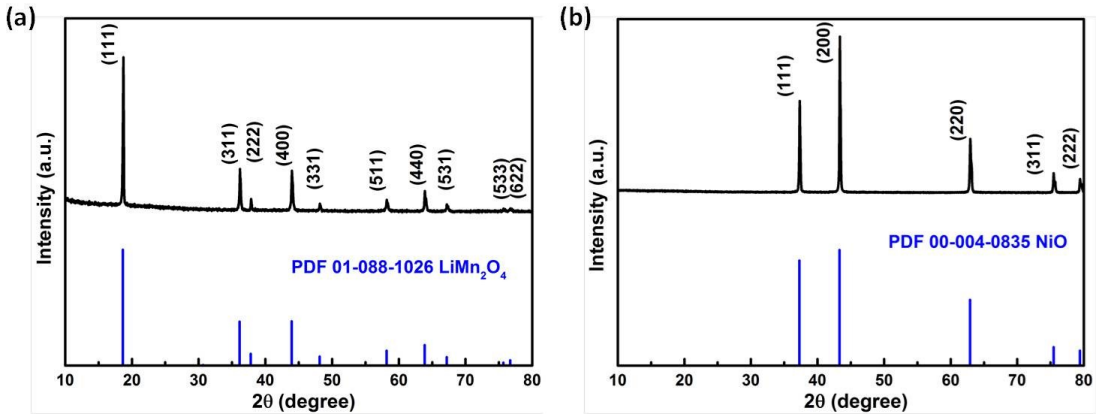

Fig. S4 XRD pattern of (a) cubic $LiMn_2O_4$ and (b) cubic NiO.

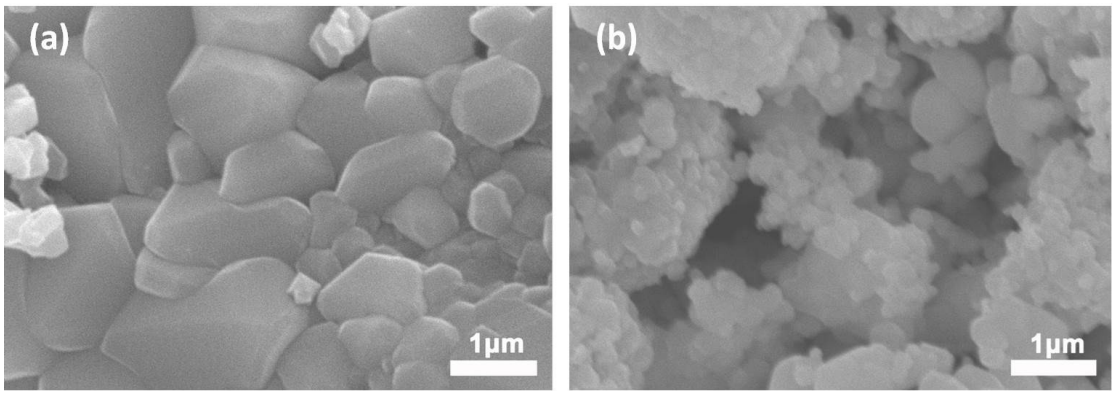

Fig. S5 FE-SEM images of (a) cubic $LiMn_2O_4$ and (b) cubic NiO.

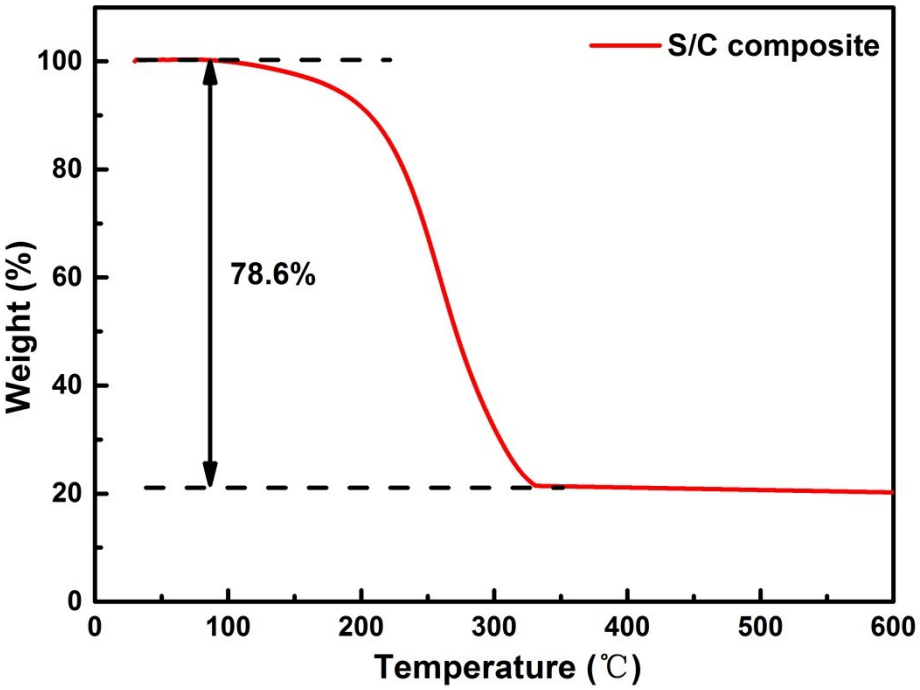

Fig. S6 TGA of S/C composite in Ar_2 at a heating rate of 10 °C min^{-1}.

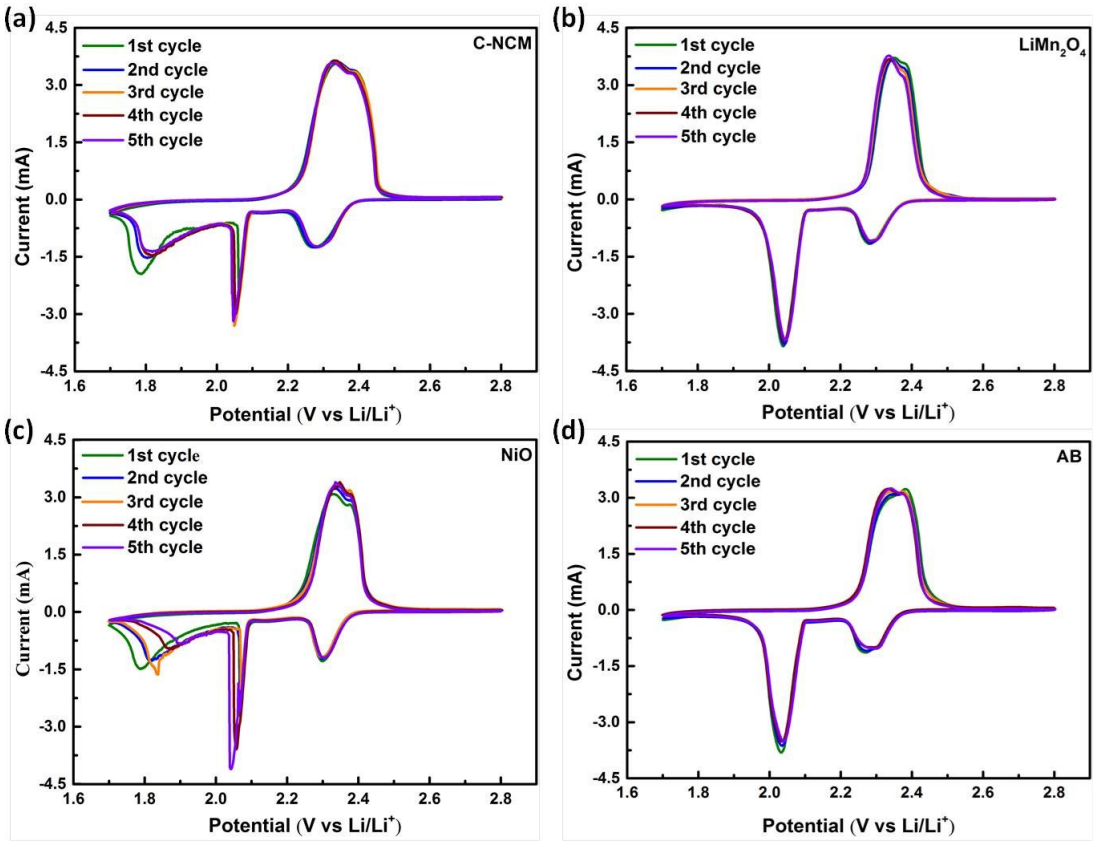

Fig. S7 CV curves for the (a) C-NCM, (b) $LiMn_2O_4$, (c) NiO and (d) AB coated separators during the first five cycles at a scan rate of 0.1 mV s^{-1}.

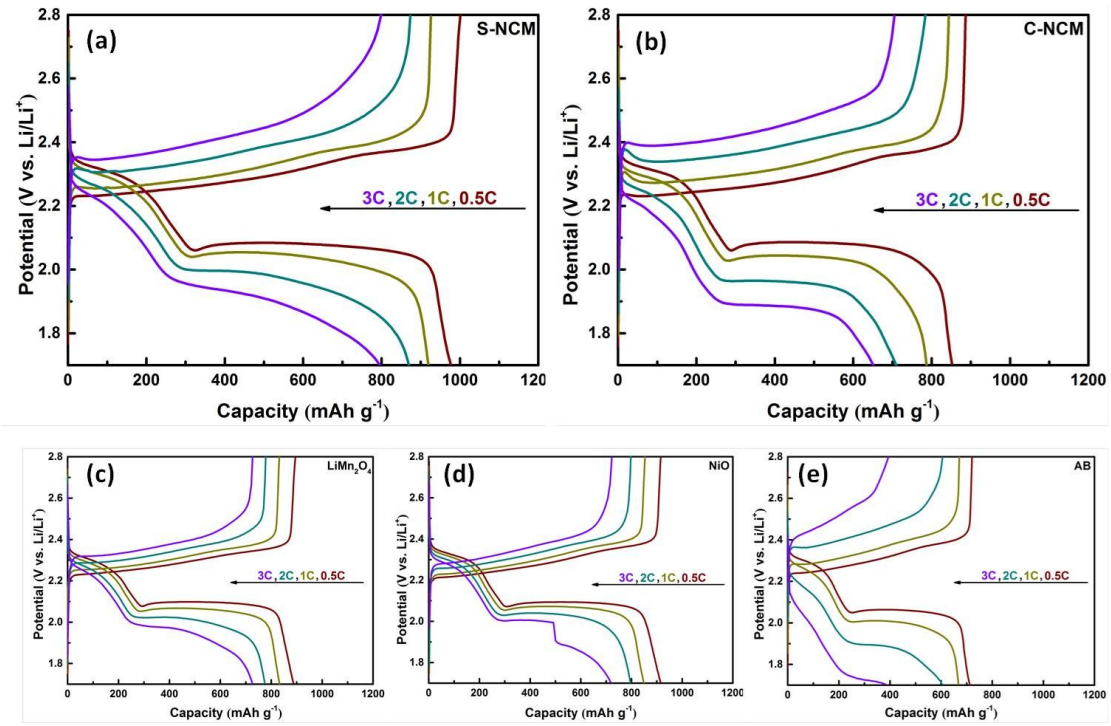

Fig. S8 Charge–discharge curves of the cells of the (a) S-NCM, (b) C-NCM, (c) $LiMn_2O_4$, (d) $LiMn_2O_4$ and (e) AB coated separator at various rates.

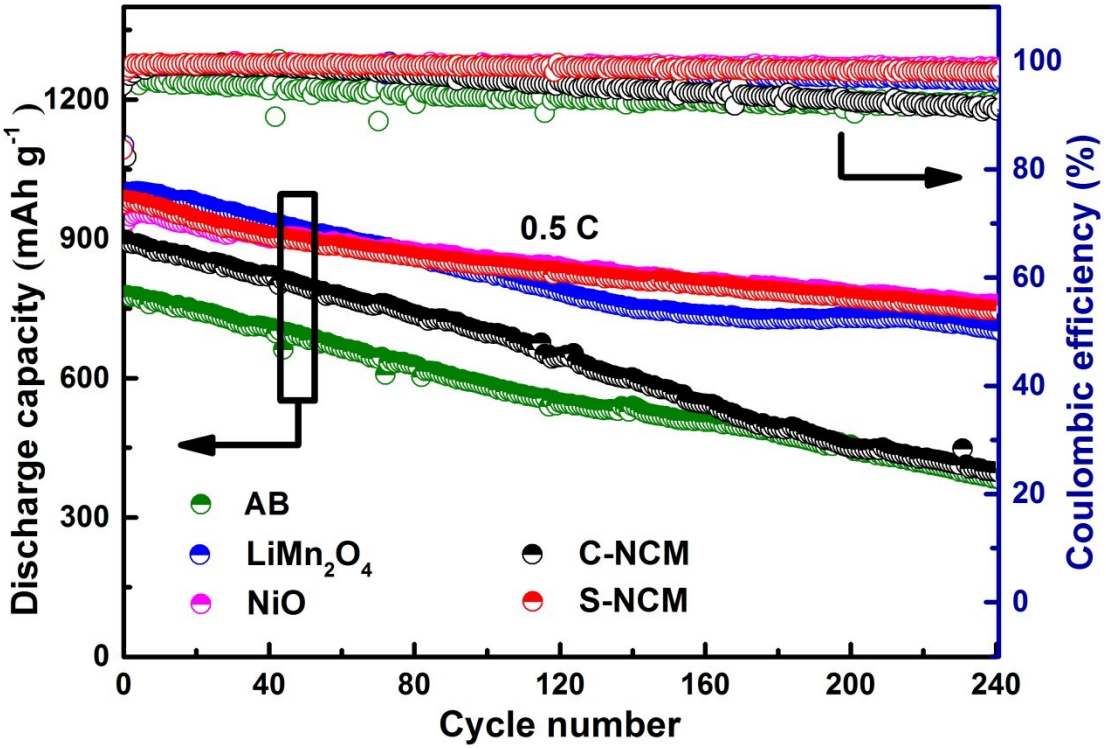

Fig. S9 Cycle performance of the Li–S cells with five different separators at 0.5 C rate.

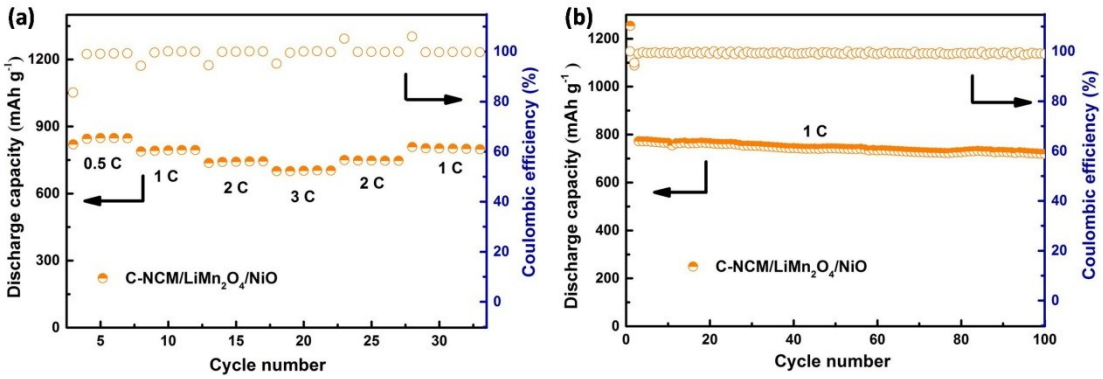

Fig. S10 (a) Rate capacities at various current densities from 0.5 to 3 C. (b) Cycle performance at 1 C rate.

Table S4 Comparison of the electrochemical performances of multi-phase composite S-NCM with pure phase metal oxides at the same conditions.

Materials	Sulfur loading (mg cm^{-2})	0.5 C (mAh g^{-1})	1 C (mAh g^{-1})	2 C (mAh g^{-1})	3 C (mAh g^{-1})	Cycle performance
S-NCM (this work)	2.21	976.1	916.7	865.2	795.1	a low fading rate of 0.053% per cycle over 550 cycles at 1 C rate.
"Bird-Nest" Structured Co_3O_4[1]	1.5	1017	788	589	-	0.064% per cycle over 550 cycles at 1 C rate.
Ni-Fe layered double hydroxide[2]	3.0	853	801	633	-	0.04% per cycle over 1000 cycles at 1 C rate.
Co_3O_4 nanoneedle[3]	4.1	1010	830	610	-	0.06% per cycle over 280 cycles at 1 C rate.
$LiNi_{0.85}Co_{0.15}Al_{0.05}O_2$[4]	3.3	994	864	<720	<640	0.02% per cycle over 500 cycles at 1 C rate.

$LiMn_2O_4$[5]	1.5	<800	<700	570	-	0.071% per cycle over 300 cycles at 0.5 C rate.
MnO_2 nanoparticles[6]	1.5-2.5	903	833	742	689	0.059% per cycle over 500 cycles at 0.5 C rate.
$NiCo_2O_4$ nanofiber[7]	1.3-1.5	872	<790	<650	<600	0.065% per cycle over 400 cycles at 0.5 C rate.
SnO_2[8]	1.0-2.0	<720	<660	<400	-	0.064% per cycle over 500 cycles at 0.2 C rate.
Co_3O_4[9]	1.0	747	647	466	423	0.066% per cycle over 550 cycles at 0.5 C rate.
Mn_2O_3[9]	1.0	<750	<700	<500	<500	0.071% per cycle over 550 cycles at 0.5 C rate.
$Co(OH)_2$[10]	0.4	1050	920	805	-	0.10% per cycle over 450 cycles at 2 C rate.
$Li_4Ti_5O_{12}$[11]	1.8-2.3	<900	<800	<720	<600	0.018% per cycle over 500 cycles at 1 C rate.
TiO_2[12]	-	889	770	714	677	0.36% per cycle over 120 cycles at 1 C rate.

Table S5 Comparison of the electrochemical performances of multi-phase composite S-NCM with two-phase composites at the same conditions.

Materials	Sulfur loading (mg cm^{-2})	0.5 C (mAh g^{-1})	1 C (mAh g^{-1})	2 C (mAh g^{-1})	3 C (mAh g^{-1})	Cycle performance
S-NCM (this work)	2.21	976.1	916.7	865.2	795.1	a low fading rate of 0.053% per cycle over 550 cycles at 1 C rate.
CoO/Co[13]	2.8-3.2	828.5	753.9	684.3	-	0.043% per cycle over 300 cycles at 1 C rate.
NiO-$NiCo_2O_4$ heterostructure[14]	-	920	821.7	697.9	-	0.059% per cycle over 500 cycles at 0.5 C rate.
$LiNO_3/Al_2O_3$[15]	0.53	1010	830	610	-	0.34% per cycle over 100 cycles at 200 mA g^{-1}.

The multi-phase composite S-NCM almost have the best rate performance among above materials including pure phase metal oxides and two-phase composites , and the cycle performance is superior to most of the materials.

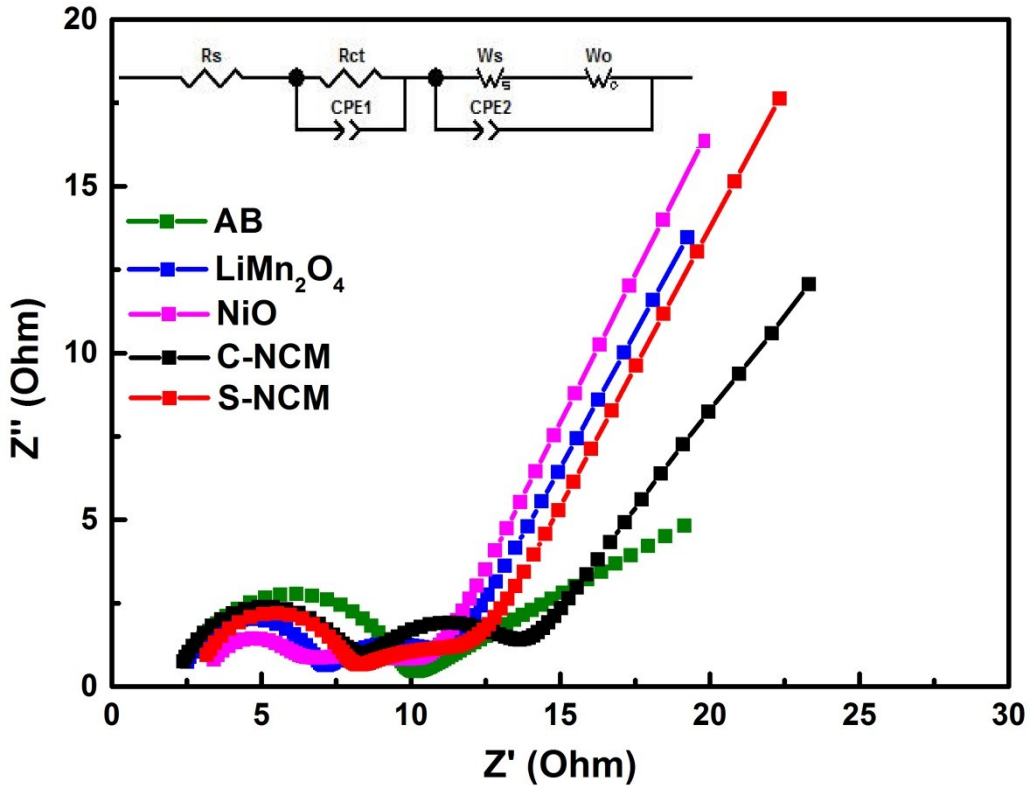

Fig. S11 EIS Nyquist plots of the cells before cycling.

Table S6 Impedance parameters of the Li-S coin cells with the five different separators before charge/discharge cycling obtained from the simulation using equivalent circuit models.

Sample	R_s/Ω	R_{ct}/Ω	W_s/Ω	W_o/Ω
AB	2.17	7.399	175.3	76.65
$LiMn_2O_4$	2.241	4.628	4.083	1.28
NiO	2.84	2.419	5.083	2.296
C-NCM	2.026	5.432	6.923	97.89
S-NCM	2.754	4.896	4.7	1.821

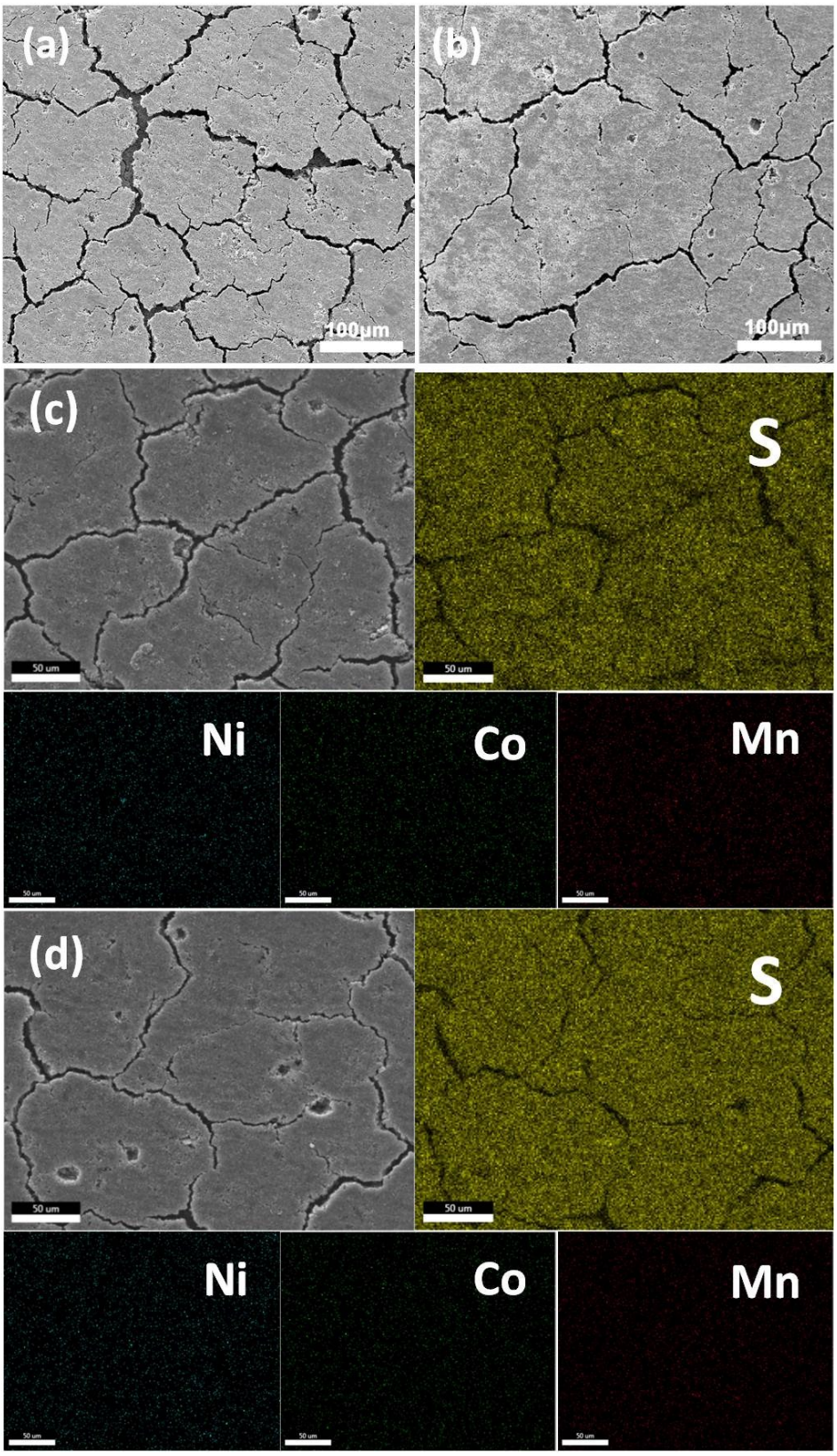

Fig. S12 SEM and element mapping of the separator evaluated from the cells after cycling at 0.5 C for 100 cycles. SEM image of the cycled (a) C-NCM and (b) S-NCM coated separator. Element mapping of the cycled (c) C-NCM and (d) S-NCM coated separator.

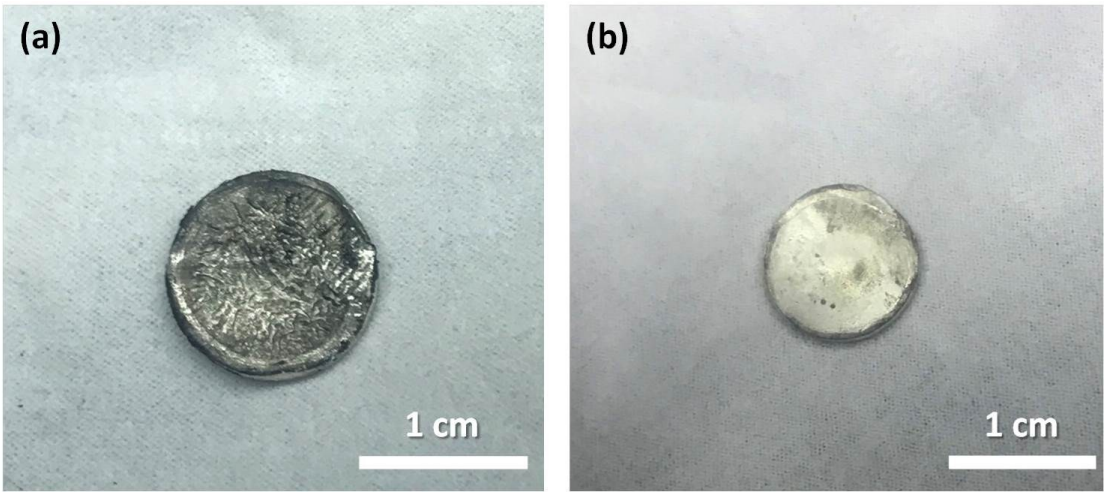

Fig. S13 The lithium metal anodes of the cells with (a) C-NCM and (b) S-NCM coated separator composite after cycling.

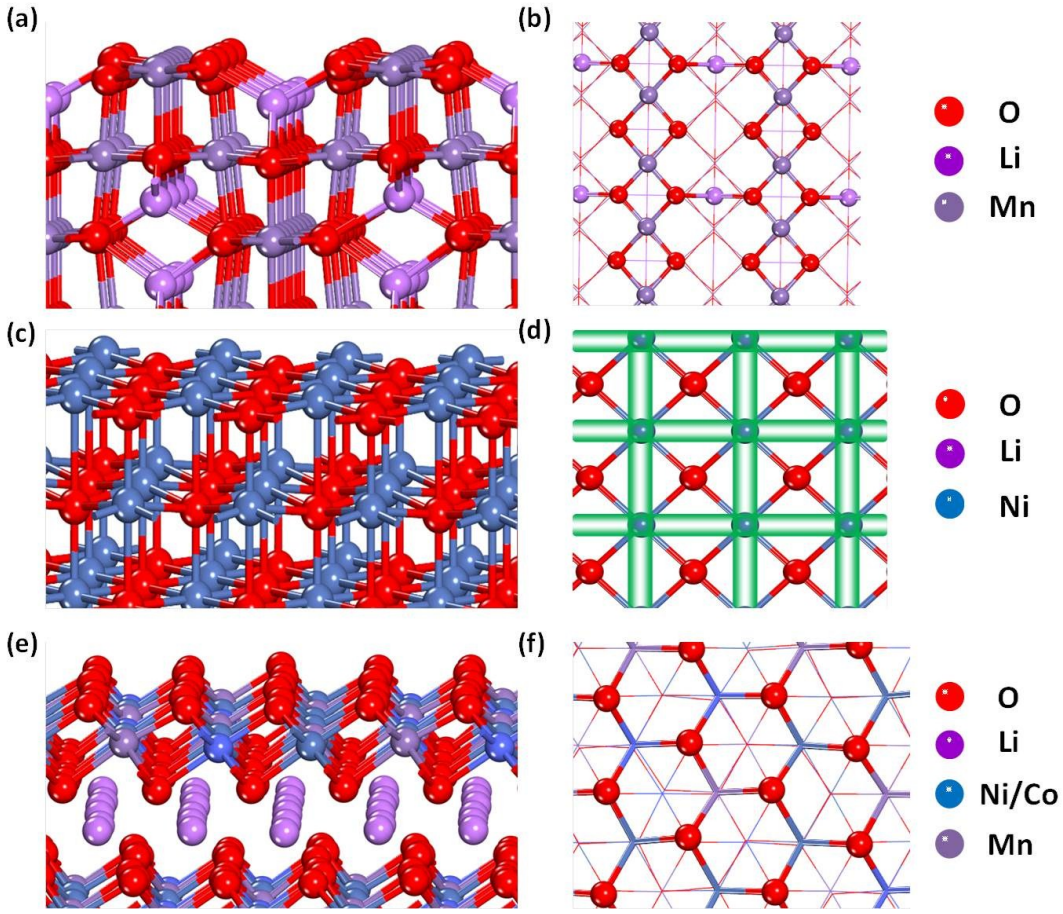

Fig. S14 The side view and top view of (a, b) $LiMn_2O_4$ (001), (c, d) NiO (001) and (e, f) $LiNi_{0.5}Co_{0.2}Mn_{0.3}O_2$ (001) lattice planes.

Table S7 Adsorption energy of Li_2S_6, Li_2S, S_5, and reaction heat of $Li_2S_6 \rightarrow Li_2S + S_5$ on $LiMn_2O_4$, NiO and $LiNi_{0.5}Co_{0.2}Mn_{0.3}O_2$ surface.

Sample	Li_2S_6 (eV)	Li_2S (eV)	S_5 (eV)	reaction heat (eV)
$LiMn_2O_4$	-2.44	-4.63	-1.38	-0.32
NiO	-4.50	-4.81	-3.87	-0.92
$LiNi_{0.5}Co_{0.2}Mn_{0.3}O_2$	-1.31	-3.66	-0.41	0.50

Calculation Method and Model

The Vienna Ab Initio Simulation Package (VASP)[16,17] for all the spin-polarized DFT calculations within the generalized gradient approximation (GGA) using the PBE functional formulation[18] were used in this work. Projected augmented wave (PAW)[19] pseudopotentials was employed to describe the interactions between ionic cores and valence electrons. 3 (Li), 6 (O), 6 (S), 7 (Mn), 9 (Co) and 10 (Ni) valence electrons were explicitly taken into account. The valence electronic states were expanded in plane wave basis sets with a cutoff energy of 500 eV. Partial occupancies of electronic bands were allowed with the Gaussian smearing method and a width of 0.01 eV. We also adopted the DFT-D3(BJ)[20] method to describe the dispersion effects in the system. For all of the $LiMn_2O_4$ (001), NiO (001) and $LiNi_{0.44}Co_{0.22}Mn_{0.33}O_2$ (001) stoichiometric model, the p (3×3) supercell with four O-containing layers was used and all the vacuum between slabs was 25 Å, in which a Monkhorst-Pack K-point mesh of 3×3×1 was included. During structural optimization, the bottom two layers of the slab were fixed at bulk truncated position and the top two layers and the adsorbates were fully relaxed. All the adsorption geometries were optimized until the forces on all atoms were below 0.05 eV/Å. The adsorption energy, E_{ads}, of the Li2S, L2S6 and S5 on the Li-ion battery is calculated as $E_{ads} = E_{M/surf} - E_{surf} - E_M$, where $E_{M/surf}$ and E_{surf} are the total energy of the Li-ion battery with and without the Li_2S, Li_2S_6 and/or S_5, respectively, and E_M is the energy of the Li_2S, L_2S_6 and S_5 in vacuum. Based on the above definition, a negative E_{ads} indicates that the adsorption is exothermic and that the adsorbent–Li_xS_y system is stable.

References

1. R. Liu, F. Guo, X. Zhang, J. Yang, M. Li, W. Miaomiao, H. Liu, M. Feng and L. Zhang, *ACS Appl. Energy Mater.*, 2019, **2**, 1348-1356.
2. J. T. Zhang, Z. Li, Y. Chen, S. Y. Gao and X. W. Lou, *Angew. Chem. Int. Edit.*, 2018, **57**, 10944-10948.
3. Z. Chang, H. Dou, B. Ding, J. Wang, Y. Wang, X. Hao and D. R. MacFarlane, *J. Mater. Chem. A*, 2017, **5**, 250-257.
4. K. Shi, C. Lai, X. Liu, Y. Wei, W. Lv, J. Wang, J. Li, C. Yan, B. Li, Q.-H. Yang, F. Kang and Y.-B. He, *Energy Storage Mater.*, 2018, DOI: 10.1016/j.ensm.2018.07.024.
5. P. H. Ji, T. B. Zeng, X. B. Hu, Y. L. Xu and G. P. Zhou, *Solid State Ionics*, 2018, **315**, 52-58.
6. X. Song, G. P. Chen, S. Q. Wang, Y. P. Huang, Z. Y. Jiang, L. X. Ding and H. H. Wang, *ACS Appl. Mater. Inter.*, 2018, **10**, 26274-26282.
7. Y.-T. Liu, D.-D. Han, L. Wang, G.-R. Li, S. Liu and X.-P. Gao, *Adv. Energy Mater.*, 2019, DOI: 10.1002/aenm.201803477, 1803477.
8. Y. Y. Xiang, Z. Wang, W. J. Qiu, Z. R. Guo, D. Liu, D. Y. Qu, Z. Z. Xie, H. L. Tang and J. S. Li, *J. Membrane Sci.*, 2018, **563**, 380-387.
9. F. Ma, J. S. Liang, T. Y. Wang, X. Chen, Y. N. Fan, B. Hultman, H. Xie, J. T. Han, G. Wu and Q. Li, *Nanoscale*, 2018, **10**, 5634-5641.
10. Y. Yang, L. Zhang, H. Xu, X. Qin, Y. Deng and G. Chen, *ACS Sustain. Chem. Eng.*, 2018, **6**, 17099-17107.
11. T. B. Zeng, X. B. Hu, P. H. Ji, B. Shang, Q. M. Peng, Y. Y. Zhang and R. Q. Song, *J. Power Sources*, 2017, **359**, 250-261.
12. H. Wang, S. Li, D. Li, Z. Chen, H. K. Liu and Z. Guo, *Energy*, 2014, **75**, 597-602.
13. W. C. Ren, W. Ma, M. M. Umair, S. F. Zhang and B. T. Tang, *Chemsuschem*, 2018, **11**, 2695-2702.
14. L. Y. Hu, C. L. Dai, H. Liu, Y. Li, B. L. Shen, Y. M. Chen, S. J. Bao and M. W. Xu, *Adv. Energy Mater.*, 2018, **8**.
15. Y. P. Guan, A. B. Wang, S. Liu, Q. Li, W. K. Wang and Y. Q. Huang, *J. Alloy. Compo.*, 2018, **765**, 544-550.
16. G. Kresse and J. Furthmüller, *Physi. Rev. B*, 1996, **54**, 11169-11186.
17. G. Kresse and J. Furthmüller, *Comp. Mater. Sci.*, 1996, **6**, 15-50.
18. J. P. Perdew, K. Burke and M. Ernzerhof, *Phys. Rev. Lett.*, 1996, **77**, 3865-3868.
19. G. Kresse and D. Joubert, *Physi. Rev. B*, 1999, **59**, 1758-1775.
20. S. Grimme, S. Ehrlich and L. Goerigk, *J. Comput. Chem.*, 2011, **32**, 1456-1465.